

Synthesis and Properties of Materials for Hydrogen Separation Membranes

Robert D. Carneim

Oak Ridge National Laboratory, 1 Bethel Valley Road, P.O. Box 2008, MS 6068, Oak Ridge, TN 37831
eMail: carneimrd@ornl.gov; Telephone: 865.574.5601; Fax: 865.574.8445

Timothy R. Armstrong

Oak Ridge National Laboratory, 1 Bethel Valley Road, P.O. Box 2008, MS 6064, Oak Ridge, TN 37831
eMail: armstrongt@ornl.gov; Telephone: 865.574.7996; Fax: 865.574.4357

Manuscript

Introduction

Hydrogen permeable materials (proton conductors) find many uses in energy applications—in particular, fuel processing. For example, dense membranes that allow the diffusion of hydrogen can be used to separate hydrogen from gas mixtures or remove hydrogen after alkane dehydrogenation (figure 1). At low temperatures ($< \approx 200$ °C) materials such as most acids and certain polymers exhibit useful conductivities. If the process requires higher temperatures (e.g., 400 °C to 1200 °C)—such as when processing a high-temperature gas where it is undesirable to cycle down in temperature pass through the hydrogen separation membrane and then back up in temperature—materials options become more limited and the application's environmental parameters suggest the use of ceramics (figure 2).

Many perovskite-based oxides are permeable to hydrogen ions, by way of OH^- migration on oxygen sites, under certain conditions making them, effectively, proton conductors.¹⁻⁵ Yttrium-doped barium cerate ($\text{BaCe}_{0.80}\text{Y}_{0.20}\text{O}_{3-\delta}$) has one of the highest conductivities of such materials (figure 2) and is the focus of this study. A critical issue that must be addressed with this material is its tendency to decompose into BaCO_3 and simple oxides in a CO_2 -containing environment at certain temperatures.⁶⁻⁸ Approaches investigated to mitigate this problem were producing slightly A-site (barium) deficient compositions and partially substituting Zr for Ce. Three solution-based synthesis methods were investigated to produce this material for further characterization. The glycine-nitrate combustion synthesis (GNP-CS) process was studied in detail in both its traditional form and a modified form in which the precursor was homogeneously dried before initiating the combustion reaction. Homogeneous coprecipitation was also examined as a non-combustion-based alternative.

Stability in CO_2

The stability of $\text{BaCe}_{0.80}\text{Y}_{0.20}\text{O}_{3-\delta}$ in a CO_2 -containing environment was evaluated since barium-containing compounds are prone to form BaCO_3 at high temperature in the presence of CO_2 . Varying the barium (A-site) stoichiometry and substituting Zr for a fraction of the Ce were investigated as means of improving the CO_2 -stability of this family of materials. High-temperature x-ray diffraction (HTXRD) in pure flowing CO_2 was used to determine at what temperature BaCO_3 formed.

Four compositions of $\text{Ba}_x\text{Ce}_{1-x}\text{Y}_{0.20}\text{O}_{3-\delta}$ powders were synthesized with $x = 0.90, 0.95, 0.98, \text{ and } 1.00$. A small sample of each powder was placed on the platinum heater strip in the HTXRD sample chamber and heated to over 1200 °C in air or flowing inert gas. After determining that the sample was single-phase perovskite under these conditions, the atmosphere was switched to flowing CO_2 . After a five-minute hold, an XRD scan was performed. On completion of the scan, the temperature was lowered by 50 °C and the process (hold at temperature \rightarrow scan \rightarrow lower temperature) repeated until the sample was fully decomposed or the temperature was down to ≈ 700 °C.

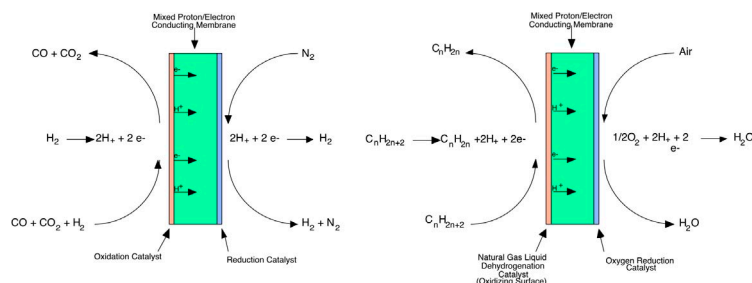


Fig. 1. Applications for protonic-electronic conducting membranes. Left: hydrogen separation; Right: alkane dehydrogenation.

It was determined that a barium deficient composition resulted in slightly better resistance to decomposition in CO_2 (the materials was stable to lower temperatures) (figure 3). Since no dependence on the degree of barium deficiency was observed, it was decided to use the composition $\text{Ba}_{0.98}\text{Ce}_{0.80}\text{Y}_{0.20}\text{O}_{3-\delta}$ (BCY88) for the bulk of this study (synthesis and characterization). This degree of barium deficiency ensured that there would be no A-site excess while minimizing the potential conductivity loss associated with more significant A-site deficiency.

The compound BaZrO_3 also has a perovskite-based structure and is nearly unaffected by CO_2 in the environment. It is possible to form solid solutions of BaZrO_3 and BaCeO_3 . The effect of adding BaZrO_3 to BaCeO_3 is increasing resistance to carbonate formation and decreasing conductivity. In the case of the undoped stoichiometric compounds, a Zr_{Ce} substitution of ≈ 0.20 is required to stabilize the material against decomposition in CO_2 . This work examined the effect of Zr_{Ce} substitution for the case of undoped A-site deficient material and then the doped A-site deficient composition. Three compositions of $\text{Ba}_{0.98}\text{Ce}_{1-x}\text{Zr}_x\text{O}_{3-\delta}$ were prepared with $x = 0.05, 0.10,$ and 0.15 and studied by HTXRD in flowing CO_2 as described above. It was found that the presence of Zr prevented complete decomposition in all three cases. The $\text{Ba}_{0.98}\text{Ce}_{0.85}\text{Zr}_{0.15}\text{O}_{3-\delta}$ composition, however, showed no carbonate formation at any temperature tested. This level of Zr_{Ce} substitution was then applied to the doped material (producing $\text{Ba}_{0.98}\text{Ce}_{0.65}\text{Zr}_{0.15}\text{Y}_{0.20}\text{O}_{3-\delta}$). High temperature XRD in CO_2 showed that BaCO_3 did form; however, this material was significantly more stable than the Zr-free composition (BCY88) with BaCO_3 disappearing above $\approx 875^\circ\text{C}$ (figure 4).

Synthesis

Solid Intermediate Glycine-Nitrate Process

Initial combustion synthesis experiments were carried out using a modified glycine-nitrate process (GNP). In standard GNP, an aqueous solution containing glycine and the appropriate amounts of metal nitrates is prepared and heated until the excess water has boiled away and the remaining material ignites—the ash and smoke resulting from this reaction being the desired ceramic phase. This process was modified in order to study the effects of various parameters in detail. The principal modification involved isolating the drying and reaction stages: after preparing the solution, it was carefully dried to produce a homogeneous solid precursor. Drying the solution proceeded in three stages: Most of the excess water was removed by moderate heating on a hot plate while stirring. Then, while the material was still fluid, the mixture was poured onto a flat, heated glass plate and manually stirred until it was almost completely dry. Finally, after cooling, the solid mass was scrapped off the glass plate and placed in a desiccator for several days. The resulting solid precursor material could then be ignited by placing it on a hot plate at $\geq 400^\circ\text{C}$ (figure 5). Material prepared thusly should result in a cleaner, higher-temperature reaction producing a more homogeneous product as compared to standard GNP.

Further modifications involved using different fuels and oxidizing metal sources (salts). The solid intermediate GNP (SIGNP) described above was used to screen the various fuel-oxidizer combinations under “best-case-scenario” reaction conditions. The four different fuels studied were gly-

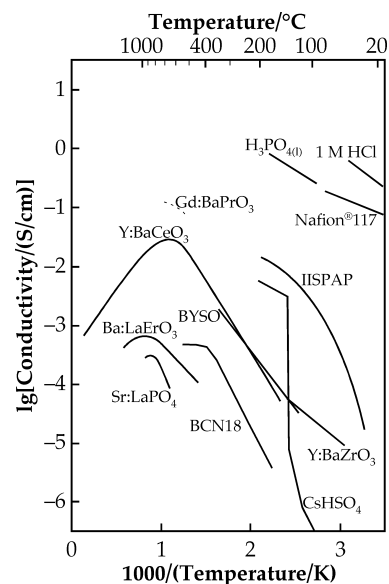


Fig. 2. Conductivity versus temperature for various proton conducting materials.⁹

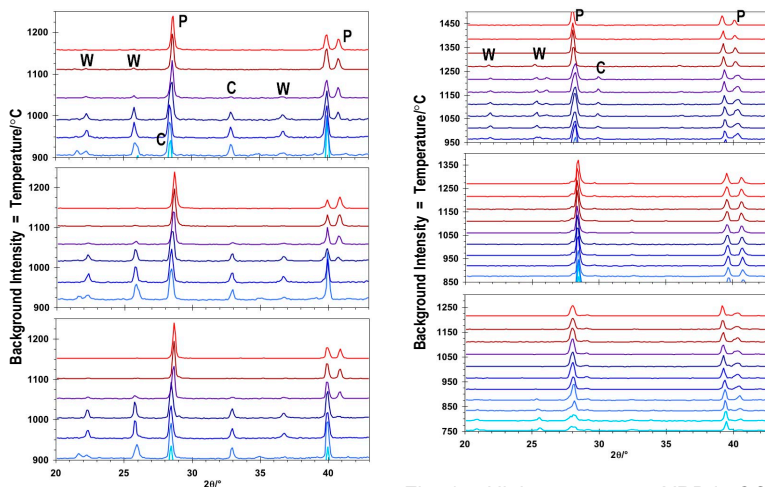


Fig. 3. High-temperature XRD in CO_2 of $\text{Ba}_x\text{Ce}_{1-x}\text{Y}_x\text{O}_{3-\delta}$ with $x = 1.00$ (top), 0.98 (center), and 0.90 (bottom). Peak legend: P = perovskite; W = BaCO_3 ; C = Ce(Y)O_2 .

Fig. 4. High-temperature XRD in CO_2 of $\text{Ba}_{0.98}\text{Ce}_{1-x}\text{Zr}_x\text{O}_{3-\delta}$ with $x = 0.05$ (top), 0.15 (center); and $\text{Ba}_{0.98}\text{Ce}_{0.65}\text{Zr}_{0.15}\text{Y}_{0.20}\text{O}_{3-\delta}$ (bottom). Peak legend: P = perovskite; W = BaCO_3 ; C = Ce(Y)O_2 .

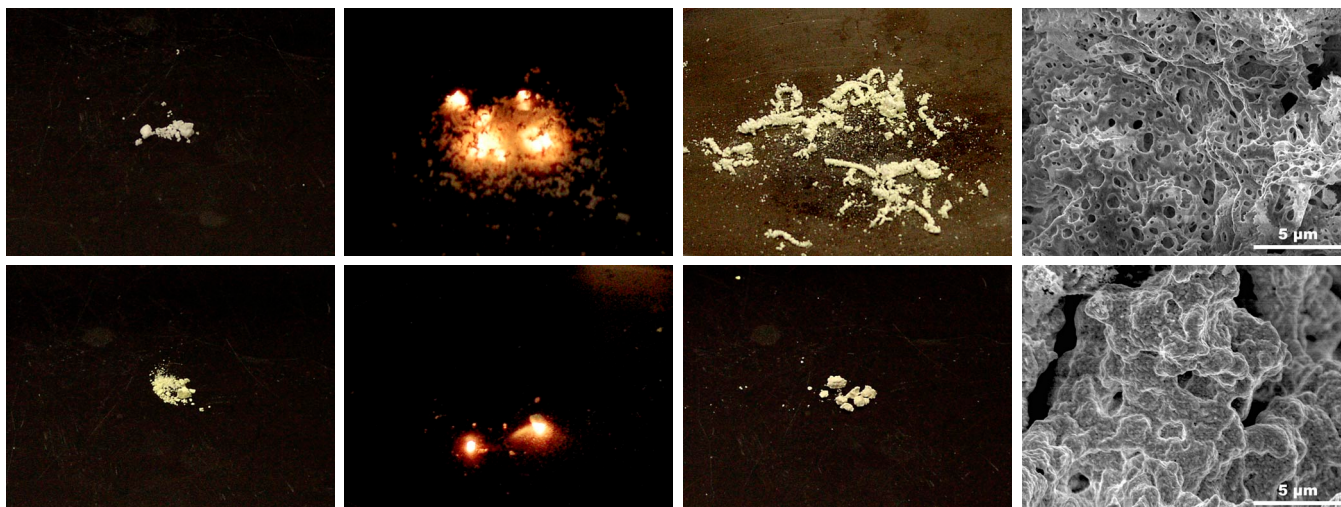


Fig. 5. Images showing the solid-intermediate combustion synthesis process utilizing standard metal nitrates as the cation sources and glycine (top) and oxalic dihydrazide (bottom) fuels: dried solid precursor (far left); reaction in progress (left-center); powder mass after completed reaction (right-center); and scanning electron micrographs of the product powder (far right).

cine, urea, carbohydrazide (CZ), and oxalic dihydrazide (ODH). The different metal source combinations used were $\text{Ba}(\text{NO}_3)_2 + \text{Ce}(\text{NO}_3)_3 + \text{Y}(\text{NO}_3)_3$; $\text{Ba}(\text{NO}_3)_2 + \text{Y}(\text{NO}_3)_3 + (\text{NH}_4)_2\text{Ce}(\text{NO}_3)_6$; and $\text{Ba}(\text{NO}_2)_2 + \text{Ce}(\text{NO}_3)_3 + \text{Y}(\text{NO}_3)_3$. The first combination is the standard composition used for GNP (the N in GNP), the second combination increases the amount of reactants and product gasses, and the final combination slightly decreases the amount of reactants and product gasses. This resulted in an initial matrix of 12 precursor compositions. In all cases, materials were batched to produce a stoichiometric combustion reaction (burn)—producing, theoretically, only N_2 , H_2O , CO_2 and BCY88. A theoretically perfect burn does not generally occur in practice. Interference from the ambient environment (O_2 and CO_2 in the air) and insufficient reaction temperatures result in incomplete combustion producing various solid phases (e.g., BaCO_3 , $\text{Ba}[\text{NO}_3]_3$, and CeO_2) and potentially NO_x or CO gasses. The 12 powders produced with this method were evaluated by pressing and sintering pellets from the as-burned powder (i.e., without any calcination or milling operation) and assessing the quality of the sintered samples.

Several trends were immediately evident while reacting (or attempting to react) the solid precursors: The urea-fueled compositions would not ignite to form a self-sustaining reaction at temperatures attainable on the hot plate ($\approx 400^\circ\text{C}$). (Though these compositions were essentially eliminated for this reason, they were reacted by placing them in a furnace at 500°C and evaluated for completeness.) The glycine-fueled compositions easily formed self-sustaining reactions producing a voluminous, low-density product powder. The CZ- and ODH-fueled compositions burned vigorously with a hotter colored flame than the glycine-fueled compositions and produced a higher-density product.

Further differences in the behavior of these powders became unmistakable while examining the sintered pellets produced from the as-burned powders (figure 6). Compositions using $\text{Ba}(\text{NO}_2)_2$ resulted in significantly warped pellets—likely due to the large disparity in crystallite size between the barium compounds and cerium/yttrium compound in the as-burned powder (XRD peaks of the ceria phase were clearly significantly broader than the barium phases) and therefore possibly enhanced reaction with the alumina setter material. Urea-fueled compositions did not densify, but were mechanically and chemically stable. Carbohydrazide-fueled samples densified well; however cracks appeared shortly after sintering and the pellets disintegrated further with time. Both the glycine-fueled and the ODH-fueled compositions, utilizing all-nitrate-metal-sources or nitrates-plus- $(\text{NH}_4)_2\text{Ce}(\text{NO}_3)_6$, sintered very well: these pellets had the highest sintered densities of the 12 compositions tested and they remained chemically stable (they did not disintegrate at ambient conditions). The ODH-fueled samples produced slightly higher quality pellets than the glycine-fueled compositions—slightly higher density and apparently more homogeneous (fewer and smaller color variations were visible on the sintered surfaces). The poor behavior of the urea- and CZ-fueled powders is likely related to the presence of a significant quantity of $\text{Ba}(\text{NO}_3)_2$, and the superior behavior of the ODH-fueled powder is related to the presence of a measurable amount of the desired final perovskite phase (figure 7).

Based on these observations, four precursor compositions were chosen for synthesis by the standard glycine-nitrate-type process and more detailed characterization. The compositions chosen were those fueled by glycine and ODH, and using all-nitrate-metal-sources and nitrates-plus- $(\text{NH}_4)_2\text{Ce}(\text{NO}_3)_6$:

- Ba-, Y-, Ce- nitrates + ODH
- Ba-, Y-, Ce- nitrates + glycine
- Ba-, Y-, nitrates + $(\text{NH}_4)_2\text{Ce}(\text{NO}_3)_6$ + ODH
- Ba-, Y-, nitrates + $(\text{NH}_4)_2\text{Ce}(\text{NO}_3)_6$ + glycine.

Standard Glycine-Nitrate Process

The four precursor compositions listed above were prepared by the standard GNP-type process as follows. Aqueous solutions were prepared containing appropriate amounts of fuel and metal salts. Due to the lower solubility of ODH (relative to glycine), these precursor solutions were necessarily more dilute and required heating during preparation. A 4 L stainless steel beaker was placed on a hot plate at its highest heat setting and preheated. For each composition, only a small amount (50 mL to 200 mL) of the total precursor batch was reacted at a time by pouring it into the stainless steel beaker, covering the beaker with a 100-mesh sieve (to contain the product), and waiting for the excess water to evaporate and the precursor to ignite (figure 8). After each sub-batch finished burning, the material produced was collected and the next sub-batch poured into the stainless steel beaker.

Homogenous Coprecipitation

Homogenous coprecipitation (HCP) was used as a third, non-combustion-based, alternative synthesis method. This technique also has the advantage of providing atomic-scale mixedness of the precursor in order to minimize thermal requirements during synthesis and produce nanocrystalline powder. A homogeneous mixed-metal oxalate precipitate was formed as follows. An aqueous solution of the appropriate mixture of metal nitrates was prepared at room temperature. Then an ammonium oxalate solution was prepared and heated to 70 °C with the total number of oxalate ions in this solution being 3 times the total number of metal ions in the metal nitrate solution. The metal nitrate solution was added rapidly, but drop-wise, to the agitated oxalate solution, pausing from time to time to allow the oxalate solution (now containing some metal nitrates and metal oxalate precipitates) temperature to return to 70 °C. After the entire metal nitrate solution was consumed, the resulting mixture was allowed to remain at 70 °C for 30 min with stirring. Then heating was discontinued and the mixture allowed to cool overnight with stirring. The precipitate was washed with deionized water several times and placed in a glass pan for drying in an oven between 50 °C and 75 °C.

It was necessary to determine a reasonable temperature at which to convert the mixed-metal oxalate to the desired single-phase oxide. High temperature powder XRD was performed in air with scans performed at 100 °C intervals from room temperature up to 1300 °C. It was found that the material was fully converted by 1000 °C, and an unidentified phase began to appear at 1200 °C. The bulk of the material was calcined for 1 h at 1100 °C in an alumina sagger by placing it into, and removing it from a hot furnace (figure 9).

Processing

Powders produced by the various synthesis methods were prepared for pellet production in different ways. The powders produced by SIGNP were used as-burned with only mild grinding in a mortar and pestle to break up soft agglomerates where necessary. Powders pro-

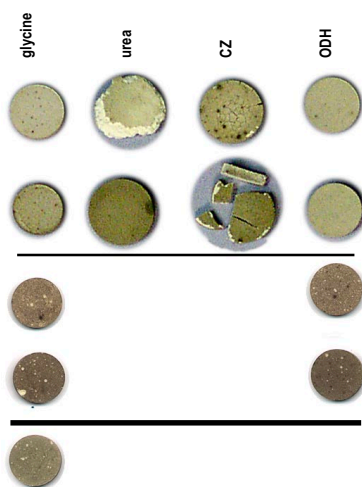


Fig. 6. Selected sintered pellets. Top two rows: prepared by SIGNP with the fuel indicated. Next two rows: prepared by standard GNP and calcined at 1200 °C. Bottom pellet: prepared by HCP.

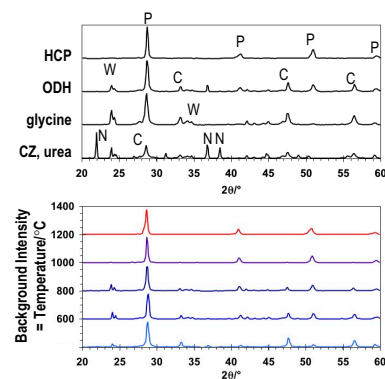


Fig. 7. Top: Powder XRD of BCY88 prepared by coprecipitation, and SIGNP using the fuels indicated. Bottom: Powder XRD of BCY88 prepared by standard GNP, ODH-fueled; as-burned and calcined at the indicated temperatures for 2 h.

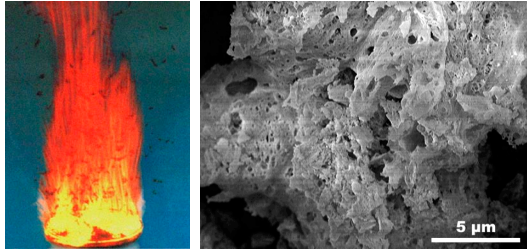


Fig. 8. Example photo of standard GNP combustion synthesis in progress (left) (the flakes of ash visible around the flame are the product) and SEM image of as-burned BCY88 produced with this method using standard metal nitrates and ODH fuel (right).

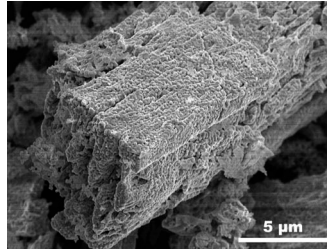


Fig. 9. SEM image of BCY88 produced by homogeneous coprecipitation, calcined 1 h at 1100 °C.

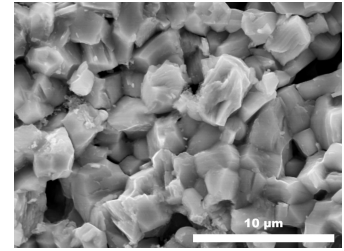


Fig. 10. SEM image of BCY88 sintered 2 h at 1550 °C.

duced by standard GNP were run through a 100-mesh sieve and calcined at various temperatures in order to ensure complete combustion and modify the phase composition of the powders. These powders were calcined in alumina saggars by placing them into a hot furnace, removing them from the furnace after a specified calcination time, and immediately dumping the powder into a cool alumina sagger to maximize the cooling rate of the powder. Calcination was carried out for 30 min at 600 °C to only eliminate any residual organics, at 1000 °C to additionally partially convert the material to the desired perovskite phase, and at 1200 °C to fully convert the powder to the desired perovskite phase. The coprecipitated powder, which had already been calcined as a necessary synthesis step, was used after running it through a 100-mesh sieve. Larger quantities of powder (i.e., 100s of grams) for future mechanical and other property characterizations were prepared using standard GNP with ODH and simple metal nitrates, sieving, and full calcination at 1200 °C (“working powder”).

Pellets were prepared by uniaxially pressing ≈ 1 g powder in a 12.7 mm diameter cylindrical steel die at ≈ 105 MPa. These pellets were then sintered at various conditions. The initial experimental matrix (12 precursor compositions prepared by SIGNP) were sintered for 10 h at 1450 °C, 1550 °C, or 1650 °C. Subsequent sintering runs were carried out at 1550 °C for 2 h (figure 10). Samples of the working powder sintered to near-full density ($> 97\%$) and were initially stable. Some samples exhibited small light-colored regions on their surfaces. Examination of the light and dark phases showed no detectable difference in the phase composition between the two by XRD (figure 11). Energy dispersive spectroscopy (EDS) indicated that the light phase had slightly higher oxygen and slightly lower cerium concentrations than the majority of the sample (dark phase), suggesting that this is a less-barium-deficient phase than the theoretical composition that has some dissolved H_2O from the environment resulting in OH^- occupying some normally vacant oxygen sites (which would be detected by EDS as a higher oxygen content) (figure 11).

Summary/Future Work

Results of high-temperature x-ray diffraction in flowing CO_2 were used as an indicator of the stability of doped barium cerate against decomposition to BaCO_3 and simple oxides. It was found that the composition $\text{Ba}_x\text{Ce}_{0.80}\text{Y}_{0.20}\text{O}_{3-\delta}$ with $0.90 \leq x \leq 0.98$ was slightly more stable than the stoichiometric composition ($x = 1.00$). Since no difference was observed between the A-site-deficient compositions tested, the composition with the smallest barium deficiency ($\text{Ba}_{0.98}\text{Ce}_{0.80}\text{Y}_{0.20}\text{O}_{3-\delta}$, BCY88) was chosen for study in order to ensure A-site deficiency while minimizing the conductivity loss associated with large barium deficiency. Substitution of Zr for some of the Ce in $\text{Ba}_{0.98}\text{CeO}_{3-\delta}$ was shown to dramatically increase its stability in CO_2 . With a Zr_{Ce} substitution in the undoped composition of 0.15, formation of BaCO_3 was undetectable in the temperature range studied (≥ 700 °C). This level of Zr_{Ce} substitution in the doped material resulted in a significant improvement in stability relative to the Zr-free composition; however, BaCO_3 formation was detected at temperatures below ≈ 875 °C.

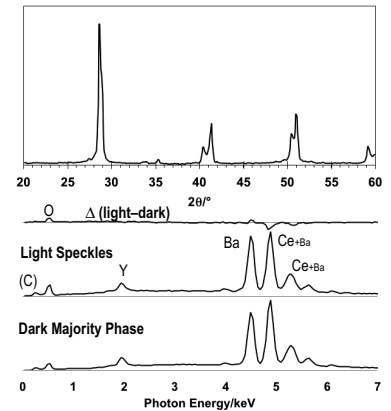


Fig. 11. Top: XRD of sintered BCY88. Bottom: EDS spectra of the majority of the sintered phase and the light-colored speckles; and the difference spectrum (light minus dark).

Three solution-based methods were studied as synthesis techniques for BCY88. Two methods were modified glycine-nitrate-type combustion synthesis processes (GNP) and the third, homogeneous oxalate coprecipitation. The GNP combustion synthesis methods were studied in detail by examining different fuels and cation sources, and, in the solid intermediate GNP (SIGNP) method, separating the drying and reaction steps of the process. Separating these steps in SIGNP resulted in a dry precursor with the fuel and oxidizer intimately and homogeneously mixed with little or no excess water. Ignition of this solid precursor necessarily resulted in a hotter—and therefore cleaner—burn, producing a more homogeneous and fully reacted powder compared to standard GNP.

The best results were obtained using the standard simple metal nitrate cation sources and either glycine or oxalic dihydrazide (ODH) as the fuel. Differences between compositions using the two fuels are slight in sintered parts, with ODH-fueled material appearing qualitatively more homogeneous. Several significant differences are apparent during the synthesis and processing stages: (1) glycine is highly soluble resulting in easy precursor solution preparation while ODH is less soluble, requiring a more dilute precursor solution and heating during preparation; (2) powders produced using ODH were more compact (higher bulk density) and therefore more easily handled and further processed than those produced using glycine, which were very low-density and porous with poor flowability; (3) ODH-fueled compositions burned at a higher temperature than those fueled by glycine, resulting in the formation of some of the desired final perovskite phase.

Future research on this material will include: (1) additional stability studies in other environments of interest including H_2O , H_2S , and further study in CO_2 utilizing thermogravimetric analysis in addition to HTXRD; (2) more in-depth characterization of the synthesized powders to gain a more fundamental understanding of the causes of the differences in behavior of the materials prepared using different synthesis methods; (3) optimizing the sintering cycle; (4) determination of the mechanical properties of BCY88 and Zr-substituted BCY88, including developing a test cell to measure mechanical strength under a chemical potential gradient; and (5) measuring the electrical properties and hydrogen permeability of BCY88 and Zr-substituted BCY88.

References

1. K. D. Kreuer, "On the Complexity of Proton Conduction Phenomena" *Solid State Ionics*, **136–37** 149–60 (2000).
2. H. G. Bohn, T. Schober, "Electrical Conductivity of the High-Temperature Proton Conductor $BaZr_{0.9}Y_{0.1}O_{2.95}$," *J. Am. Ceram. Soc.*, **83**[4] 768–72 (2000).
3. K. Katahira, Y. Yoshirou, T. Shimura, H. Iwahara, "Protonic Conduction in Zr-Substituted $BaCeO_3$," *Solid State Ionics*, **138** 91–98 (2000).
4. K. Takeuchi, C.-K. Loong, J. W. Richardson Jr., J. Guan, S. E. Dorris, U. Balachandran, "The Crystal Structures and Phase Transitions in Y-Doped $BaCeO_3$: Their Dependence on Y Concentration and Hydrogen Doping," *Solid State Ionics*, **138** 63–77 (2000).
5. K. S. Knight, "Structural Phase Transitions, Oxygen Vacancy Ordering and Protonation in Doped $BaCeO_3$: Results from Time-of-Flight Neutron Powder Diffraction Investigations," *Solid State Ionics*, **145** 275–94 (2001).
6. G. Ma, T. Shimura, H. Iwahara, "Ionic Conduction and Nonstoichiometry in $Ba_xCe_{0.90}Y_{0.10}O_{3-\alpha}$," *Solid State Ionics*, **110** 103–10 (1998).
7. D. Shima, S. M. Haile, "The Influence of Cation Non-Stoichiometry on the Properties of Undoped and Gadolinia-Doped Barium Cerate," *Solid State Ionics*, **97** 443–55 (1997).
8. K. H. Ryu, S. M. Haile, "Chemical Stability and Proton Conductivity of Doped $BaCeO_3$ - $BaZrO_3$ Solid Solutions," *Solid State Ionics*, **125** 355–67 (1999).
9. T. Norby, "Solid-State Protonic Conductors: Principles, Properties, Progress, and Prospects," *Solid State Ionics*, **125** 1–11 (1999).